Locally implicit time-domain finite element method for sound field analysis including permeable membrane sound absorbers

Yoshida, Takumi
Okuzono, Takeshi
Sakagami, Kimihiro

(Citation)
Acoustical Science and Technology,41(4):689-692

(Issue Date)
2020-07-01

(Resource Type)
journal article

(Version)
Version of Record

(URL)
https://hdl.handle.net/20.500.14094/90009298

ACOUSTICAL LETTER

Locally implicit time-domain finite element method for sound field analysis including permeable membrane sound absorbers

Takumi Yoshida[1,*], Takeshi Okuzono[2] and Kimihiro Sakagami[2]

[1]*Technical Research Institute, Hazama Ando Corporation, 515–1 Karima, Tsukuba, 305–0822 Japan*
[2]*Environmental Acoustic Laboratory, Department of Architecture, Graduate School of Engineering, Kobe University, 1–1 Rokkodai-cho, Nada-ku, Kobe, 657–8501 Japan*

(*Received 21 August 2019, Accepted for publication 31 October 2019*)

Keywords: Iterative method, Permeable membrane absorber, Room acoustics simulation, Time-domain FEM
PACS number: 43.55.Br, 43.55.Ka, 43.55.Dt [doi:10.1250/ast.41.689]

1. Introduction

In recent years, many wave-based time-domain numerical methods, which solve a wave equation numerically in both space and time with appropriate boundary conditions and initial conditions, have become available for room acoustics simulation [1–6]. Among other methods, the time-domain finite element method (TD-FEM) is inherently useful to model complex room shapes with finite element discretization in space. However, a standard formulation of TD-FEM engenders an implicit time-marching scheme. It is often regarded as a more time-consuming method than other explicit methods such as the finite-difference time domain method [1,3,5,6].

A first-order ordinary differential equation (ODE)-based TD-FEM [7,8] has been proposed recently as an alternative method to the standard implicit TD-FEM. First-order ODE-based TD-FEM shows an explicit algorithm. Additionally, it has fourth-order accuracy with respect to dispersion error under an idealized condition using a dispersion reduction technique called modified integration rules [9]. Regarding absorption boundary modeling, it uses the simplest equivalent impedance model to address sound absorption at a room's boundary surface. The equivalent impedance model, which assumes local reaction, uses constant real-valued surface impedance in the frequency ranges of interest. However, the equivalent impedance is unable to consider both the frequency-dependence and incidence-angle dependence of the sound absorption of materials accurately. In this study, we specifically examine the efficient implementation of a sound absorber model of permeable membranes (PMs) into first-order ODE-based TD-FEM to increase its accuracy.

For this study, the PMs are thin woven or nonwoven air-permeable fabrics made from various natural or chemical fibers [10–12]. They have been used effectively to control acoustics inside buildings such as in conference rooms, stadiums, and swimming pools [13]. Basic PM absorbers have both strong frequency-dependent and incident-angle-dependent absorption behavior [14]. Therefore, they cannot be modeled using the equivalent impedance model. Recently, an extended-reaction (ER) model of PMs has been implemented into implicit TD-FEM [15]. In earlier work [16], the ER model was implemented into first-order ODE-based TD-FEM straightforwardly and its validity was confirmed. However, simple implementation of the ER model engenders a fully implicit time marching scheme, which degrades the efficiency of an explicit algorithm.

The present work was undertaken to alleviate the major difficulty explained above. Consequently, we propose a locally implicit time marching scheme for the first-order ODE-based TD-FEM to predict sound fields including PM absorbers. The locally implicit scheme is realized by applying a linear equation solver locally into a linear equation with a small degree of freedom associated with PM elements. In doing so, the remaining linear system is solvable explicitly. The efficiency of the present scheme is demonstrated through two numerical examples including acoustic simulations inside a room of practical size with PM ceiling absorbers.

2. Theory

2.1. First-order ODE-based TD-FEM for acoustic simulation including PM absorbers

For this study, PMs are assumed to be limp materials with two material parameters: surface density M and flow resistance R. The applicability of the limp model can be reviewed in the author's earlier work [15]. The semidiscretized matrix equation of TD-FEM in the forms of the second-order ODE for sound field analyses including PMs is expressed as [15]

$$\boldsymbol{M}\ddot{\boldsymbol{p}} + c_0^2\left(\boldsymbol{K} + \frac{\rho_0}{M}\boldsymbol{S}\right)\boldsymbol{p} + c_0\left(\boldsymbol{C} + \frac{\rho_0 c_0}{R}\boldsymbol{S}\right)\dot{\boldsymbol{p}} = \boldsymbol{f}, \quad (1)$$

where $\boldsymbol{M}$, $\boldsymbol{K}$, and $\boldsymbol{C}$ respectively denote the global mass matrix, the global stiffness matrix, and the global dissipation matrix. The global matrix $\boldsymbol{S}$ denotes the PM contribution. Furthermore, $\boldsymbol{p}$, $\boldsymbol{f}$, and c_0 respectively signify the sound pressure vector, the external force vector, and the speed of sound. ρ_0 denotes the air density. Symbols $\cdot$ and $\cdot\cdot$ signify first-order and second-order time derivatives respectively. A diagonal mass matrix $\boldsymbol{D}$ diagonalized from $\boldsymbol{M}$ and a vector $\boldsymbol{v} = \dot{\boldsymbol{p}}$ are introduced for explicit calculation of Eq. (1). Using them, the second-order ODE of Eq. (1) is transformed into [16]

$$\boldsymbol{D}\dot{\boldsymbol{p}} = \boldsymbol{M}\boldsymbol{v}, \quad (2)$$

*e-mail: yoshida.takumi@ad-hzm.co.jp

$$\boldsymbol{D}\dot{\boldsymbol{v}} = \boldsymbol{f} - c_0^2\left(\boldsymbol{K} + \frac{\rho_0}{M}\boldsymbol{S}\right)\boldsymbol{p} - c_0\left(\boldsymbol{C} + \frac{\rho_0 c_0}{R}\boldsymbol{S}\right)\dot{\boldsymbol{p}}. \quad (3)$$

For stable computation, $\dot{\boldsymbol{p}}$ in Eq. (2) and $\dot{\boldsymbol{v}}$ in Eq. (3) are respectively discretized using the first-order accurate forward difference and backward difference. The resulting time-marching scheme is expressed as

$$\boldsymbol{p}^n = \boldsymbol{p}^{n-1} + \Delta t\boldsymbol{D}^{-1}\boldsymbol{M}\boldsymbol{v}^{n-1}, \quad (4)$$

$$\left[\boldsymbol{D} + \Delta t c_0\left(\boldsymbol{C} + \frac{\rho_0 c_0}{R}\boldsymbol{S}\right)\right]\boldsymbol{v}^n = \boldsymbol{D}\boldsymbol{v}^{n-1} + \Delta t\left[\boldsymbol{f}^n - c_0^2\left(\boldsymbol{K} + \frac{\rho_0}{M}\boldsymbol{S}\right)\boldsymbol{p}^n\right]. \quad (5)$$

In these equations, Δt and n respectively represent the time interval and the time step. Although Eq. (4) can be computed explicitly, Eq. (5) becomes implicit because the matrix $\boldsymbol{S}$ has nondiagonal components that cannot be lumped. Therefore, Eq. (5) must be solved using a linear equation solver. As the linear system solver, the conjugate gradient (CG) solver with a diagonal scaling preconditioning is used with a convergence tolerance of 10^{-6}.

2.2. Locally implicit scheme

As described above, the simple implementation of the PM model impairs the benefits of explicit computation in first-order ODE-based TD-FEM. However, this inefficiency can be alleviated by locally applying a linear system solver into a linear equation associated with the PM matrix because the nondiagonal component appears only for row-related nodes on the surface of PMs. The local linear system is quite a small part of the whole system, as shown in later numerical examples. By local application of the linear system solver, the other remaining part of the system is solvable explicitly as

$$(\boldsymbol{D} + \Delta t c_0\boldsymbol{C})\boldsymbol{v}^n = \boldsymbol{D}\boldsymbol{v}^{n-1} + \Delta t(\boldsymbol{f}^n - c_0^2\boldsymbol{K}\boldsymbol{p}^n). \quad (6)$$

Here, the dissipation matrix $\boldsymbol{C}$ must be lumped for explicit computation. This study uses a standard row sum method for the lumped matrix.

The reduction effect of computational costs by the present locally implicit scheme over the fully implicit scheme can be estimated theoretically, particularly by addressing the main numerical operation of TD-FEM, i.e., the number of sparse matrix-vector products, N_{mv}. Here, the fully implicit scheme means that Eq. (5) is applied to the whole linear system of equations. N_{mv} for the fully implicit scheme, $N_{\mathrm{mv}}^{\mathrm{full}}$, is counted as

$$N_{\mathrm{mv}}^{\mathrm{full}} = N_{\mathrm{step}} \times 2 + N_{\mathrm{iter}}, \quad (7)$$

where N_{step} and N_{iter} respectively represent the total number of time steps and the total number of iterations. The first term of Eq. (7) means N_{mv} for $\boldsymbol{M}\boldsymbol{v}$ in Eq. (4) and $(\boldsymbol{K} + \frac{\rho_0}{M}\boldsymbol{S})\boldsymbol{p}$ in Eq. (5). The second term expresses N_{mv} for the iterative operation by the CG solver. However, N_{mv} of the locally implicit scheme, $N_{\mathrm{mv}}^{\mathrm{local}}$, is counted as

$$N_{\mathrm{mv}}^{\mathrm{local}} = N_{\mathrm{step}} \times 2 + \gamma N_{\mathrm{iter}} \quad (8)$$

with the following coefficient γ:

$$\gamma = \frac{N_{\mathrm{PM}}}{N_{\mathrm{All}}}. \quad (9)$$

Here, N_{PM} and N_{All} respectively stand for the number of unknowns associated with the PM matrix and the number of unknowns of the whole system. In Eq. (8), the first term represents N_{mv} for $\boldsymbol{M}\boldsymbol{v}$ in Eq. (4) and $\boldsymbol{K}\boldsymbol{p}$ in Eq. (6). The difference between the two schemes appears in the second term of Eqs. (7) and (8). The locally implicit scheme can reduce the number of CG solver operations to γ times that of the fully implicit scheme. The computational costs can be reduced markedly using the locally implicit scheme because N_{PM} is generally much lower than N_{All}.

3. Numerical examples

The efficiency of the present locally implicit scheme is demonstrated through two numerical examples that have different sizes of problems in simulation in the architectural acoustics field: a simple impedance tube problem and an acoustic simulation inside a room of practical size. In both cases, the most classical single-leaf PM absorber, i.e., a sound-absorbing structure composed of a PM and a rigid-backed air cavity, is installed into the sound fields. Three PMs, each with a different surface density M and flow resistance R are installed: (1) PM-A with $M = 0.065\,\mathrm{kg/m^2}$, $R = 196\,\mathrm{Pa\,s/m}$; (2) PM-B with $M = 0.120\,\mathrm{kg/m^2}$, $R = 462$ Pa s/m; and (3) PM-C with $M = 0.495\,\mathrm{kg/m^2}$, $R = 1{,}087$ Pa s/m. The accuracy of the locally implicit scheme was examined by comparison with a reference solution calculated using the fully implicit scheme. Note that the reference solution does not mean a convergent solution; it was only used for verifying whether the two schemes have the same accuracy under the same mesh. In addition, the efficiency was evaluated using the following measure r:

$$r = \frac{N_{\mathrm{mv}}^{\mathrm{local}}}{N_{\mathrm{mv}}^{\mathrm{full}}}. \quad (10)$$

3.1. Impedance tube problem

Figure 1 shows an impedance tube model with a single-leaf PM absorber with an air cavity depth of 0.2 m. A source and a receiving point are respectively located at $(x, y, z) = (0.0, 0.05, 0.05)$ and $(x, y, z) = (0.45, 0.05, 0.05)$. A modulated Gaussian pulse with an upper limit frequency of 1,500 Hz is given as a volume acceleration waveform. Regarding the boundary conditions, the tube inlet is an absorbing boundary with the characteristic impedance of air and other boundaries

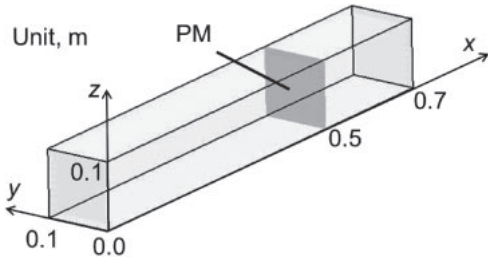

Fig. 1 Analyzed impedance tube model with a single-leaf PM absorber.

Table 1 Calculation conditions of two meshes.

Mesh	h, m	Δt, s	γ
1	0.005	1/131,000	0.014
2	0.05	1/10,400	0.143

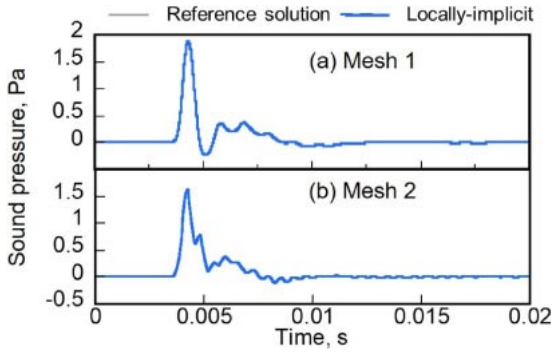

Fig. 2 Waveforms for the case with PM-C for the reference solution and locally implicit scheme with (a) Mesh 1 and (b) Mesh 2.

Table 2 r for PM-A–C using Mesh 1 and Mesh 2.

	PM-A	PM-B	PM-C
Mesh 1	0.410	0.427	0.416
Mesh 2	0.358	0.375	0.411

Table 3 Mean number of iterations for PM-A–C using Mesh 1 and Mesh 2.

	PM-A	PM-B	PM-C
Locally (Mesh 1)	17.4	13.1	9.8
Fully (Mesh 1)	4.2	3.3	2.8
Locally (Mesh 2)	3.0	3.0	3.0
Fully (Mesh 2)	4.7	4.3	3.9

are treated as rigid walls. Waveforms up to 0.1 s are calculated using two FE meshes (Mesh 1 and Mesh 2) of different mesh size and γ. Table 1 shows mesh size h, Δt, and γ for Mesh 1 and Mesh 2. The data indicate that the locally implicit scheme performs better for Mesh 1. Figure 2 presents waveforms at the receiving point for the reference solution and the locally implicit scheme calculated using Mesh 1 and Mesh 2 for the case with PM-C. Note that the waveforms of reference solution vary depending on the mesh used. Only the use of Mesh 1 causes convergence to the theoretical solution in the calculation of normal-incidence absorption coefficients [16]. In both coarse and fine meshes, the waveforms of the locally implicit scheme agree well with the reference solution. The results are also true for the other cases. Table 2 shows r for all cases. The locally implicit scheme reduces N_{mv} to 35.8–42.7% of those in the fully implicit scheme in all cases. Table 3 presents the mean number of iterations for the respective schemes. The local system is solvable in almost all cases with

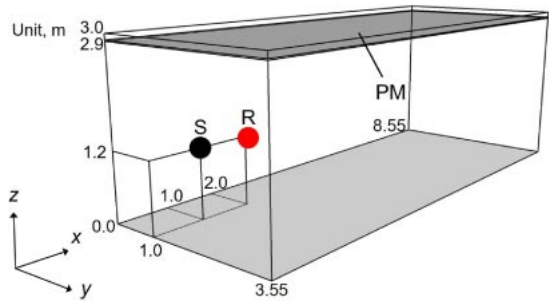

Fig. 3 Rectangular room with a PM ceiling absorber having an air cavity depth of 0.1 m, source point S, and receiver R.

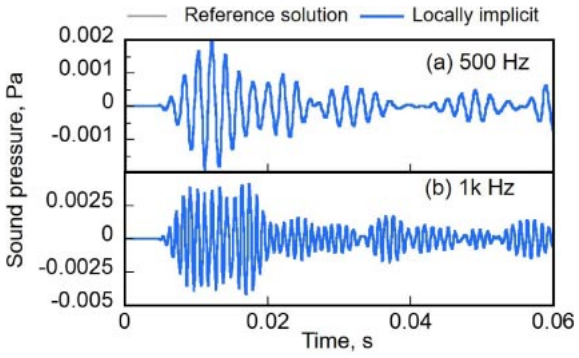

Fig. 4 Waveforms for the case with PM-C for the reference solution and the locally implicit scheme at (a) 500 Hz and (b) 1 kHz.

only a few iterations. However, when using Mesh 1, the convergence of the CG solver in the locally implicit scheme occurs much more slowly than that in the fully implicit scheme. This is an unexpected result of lower efficiency when using the fine mesh. The reason for this result is unclear and remains as a subject of future research.

3.2. Room of practical size

A sound field in a rectangular room (8.55 m long, 3.55 m wide, and 3.0 m high) with a PM ceiling absorber was analyzed to demonstrate the efficiency of a locally implicit scheme for a practical case. The air cavity depth of the absorber is 0.1 m. Figure 3 shows the analyzed rectangular room with a source point S and a receiver R. The 1/3 octave band-limited impulse responses were calculated at 500 Hz and 1 kHz with a source signal of the impulse response of an IIR filter. Regarding boundary conditions, a real-valued equivalent impedance, $z_{\mathrm{e}} = 126.3$, which corresponds to a statistical absorption coefficient of 0.059, was given to the walls and the floor. The FE mesh used here satisfies a spatial resolution of 6.1 elements per wavelength at the upper-limit frequency of the 1 kHz 1/3 octave band. In this mesh, γ equals 0.031. Impulse responses were calculated up to 2.0 s with $\Delta t = 1/10,400$ s. Figure 4 presents comparisons of waveforms up to 0.06 s between the reference solution and the locally implicit scheme in the case with PM-C. The waveforms calculated using the locally implicit scheme show good agreement with the reference solution. Figure 5 shows

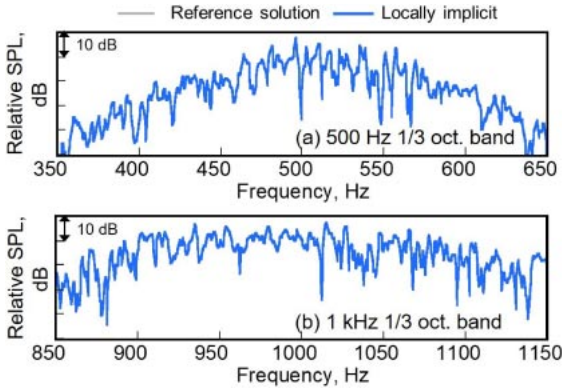

Fig. 5 Frequency characteristics at R for the case with PM-C for the reference solution and the locally implicit scheme: (a) 500 Hz 1/3 oct. band and (b) 1 kHz 1/3 oct. band.

Table 4 r for PM-A–C at 500 Hz and 1 kHz.

	PM-A	PM-B	PM-C
500 Hz	0.215	0.256	0.325
1 kHz	0.210	0.249	0.312

Table 5 Mean number of iterations for PM-A–C at 500 Hz and 1 kHz.

	PM-A	PM-B	PM-C
Locally (500 Hz)	9.3	7.2	5.8
Fully (500 Hz)	8.6	6.7	4.7
Locally (1 kHz)	9.9	7.9	6.0
Fully (1 kHz)	9.0	7.0	5.0

frequency characteristics of the reference solution and the locally implicit scheme for the case with PM-C. The locally implicit solution agrees well with the reference solution. Table 4 shows the efficiency measure r for all cases; the data indicate that the locally implicit scheme is 3.08–4.76 times faster than the fully implicit scheme. Table 5 shows the mean number of iterations for each method. For both methods, the iterative solver converges within 10 iterations.

4. Conclusion

We proposed a locally implicit TD-FEM based on a first-order ODE for simulating room acoustics in a room with PM sound absorbers. Merely by applying an iterative solver into a linear system associated with PM materials, a large portion of the linear system becomes explicitly solvable. The two numerical examples of the impedance tube problem and acoustic simulation of a practical size room demonstrated that the locally implicit scheme outperforms the fully implicit scheme without reducing accuracy.

References

[1] S. Sakamoto, H. Nagatomo, A. Ushiyama and H. Tachibana, "Calculation of impulse responses and acoustic parameters in a hall by the finite-difference time-domain method," *Acoust. Sci. & Tech.*, **29**, 256–265 (2008).
[2] T. Okuzono, T. Otsuru, R. Tomiku and N. Okamoto, "Fundamental accuracy of time domain finite element method for sound-field analysis of rooms," *Appl. Acoust.*, **71**, 940–946 (2010).
[3] R. Mehra, N. Raghuvanshi, L. Savioja, M. C. Lin and D. Manocha, "An efficient GPU-based time domain solver for the acoustic wave equation," *Appl. Acoust.*, **73**, 83–94 (2012).
[4] T. Okuzono, T. Otsuru, R. Tomiku and N. Okamoto, "Application of modified integration rule to time-domain finite-element acoustic simulation of rooms," *J. Acoust. Soc. Am.*, **132**, 804–813 (2012).
[5] S. P. Simonaho, T. Lähivaara and T. Huttunen, "Modeling of acoustic wave propagation in time-domain using the discontinuous Galerkin method: A comparison with measurements," *Appl. Acoust.*, **73**, 173–183 (2012).
[6] M. Hornikx, T. Krijnen and L. van Harten, "openPSTD: The open source pseudospectral time-domain method for acoustic propagation," *Comput. Phys. Commun.*, **203**, 298–308 (2016).
[7] T. Okuzono, T. Yoshida, K. Sakagami and T. Otsuru, "An explicit time-domain finite element method for room acoustics simulations: Comparison of the performance with implicit methods," *Appl. Acoust.*, **104**, 76–84 (2016).
[8] T. Yoshida, T. Okuzono and K. Sakagami, "Numerically stable explicit time-domain finite element method for room acoustics simulation using an equivalent impedance model," *Noise Control Eng. J.*, **66**, 176–189 (2018).
[9] B. Yue and M. N. Guddati, "Dispersion-reducing finite elements for transient acoustics," *J. Acoust. Soc. Am.*, **118**, 2132–2141 (2005).
[10] R. Pieren, "Sound absorption modeling of thin woven fabrics backed by an air cavity," *Text. Res. J.*, **82**, 864–874 (2012).
[11] K. Sakagami, T. Okuzono, Y. Somatomo, K. Funahashi and M. Toyoda, "A basic study on a rectangular plane space sound absorber using permeable membranes," *Sustainability*, **11**, 2185 (2019).
[12] M. Toyoda, K. Funahashi, T. Okuzono and K. Sakagami, "Predicted absorption performance of cylindrical and rectangular permeable membrane space sound absorbers using the three-dimensional boundary element method," *Sustainability*, **11**, 2714 (2019).
[13] T. Adams, *Sound Materials: A Compendium of Sound Absorbing Materials for Architecture and Design* (Frame Publishers, Amsterdam, 2016), 288 pages.
[14] K. U. Ingard, "Sheet absorbers," in *Notes on Sound Absorption Technology* (Noise Control Foundation, New York, 1994), Chap. 1, pp. 1-1–1-16.
[15] T. Okuzono, N. Shimizu and K. Sakagami, "Predicting absorption characteristics of single-leaf permeable membrane absorbers using finite element method in a time domain," *Appl. Acoust.*, **151**, 172–182 (2019).
[16] T. Yoshida, T. Okuzono and K. Sakagami, "A three-dimensional time-domain finite element method based on first-order ordinary differential equations for treating permeable membrane absorbers," *Proc. 25th Int. Congr. Sound Vib.*, 838, 7 pages (2018).